Nano Research
DOI 10.1007/s12274-015-0857-0
Research Article
ISSN 1998-0124
CN 11-5974/O4

Dynamic observation of oxygen vacancies in hafnia layer by *in situ* transmission electron microscopy

Chao Li[1,§], Yuan Yao[1,§], Xi Shen[1], Yanguo Wang[1], Junjie Li[1], Changzhi Gu[1], Richeng Yu[1] (✉), Qi Liu[2], and Ming Liu[2] (✉)

[1] *Beijing National Laboratory of Condensed Matter Physics, Institute of Physics, Chinese Academy of Sciences, Beijing 100190, China*
[2] *Laboratory of Nano-Fabrication and Novel Devices Integrated Technology, Institute of Microelectronics, Chinese Academy of Sciences, Beijing 100029, China*
[§] *These authors contributed equally to this work.*

Received: 12 May 2015
Revised: 24 June 2015
Accepted: 7 July 2015

KEYWORDS
charge-trapping flash,
in situ TEM,
electric field,
oxygen vacancy

ABSTRACT

The charge-trapping process, with HfO_2 film as the charge-capturing layer, has been investigated by using *in situ* electron energy-loss spectroscopy and *in situ* energy-filter image under positive external bias. The results show that oxygen vacancies are non-uniformly distributed throughout the HfO_2 trapping layer during the programming process. The distribution of the oxygen vacancies is not the same as that of the reported locations of the trapped electrons, implying that the trapping process is more complex. These bias-induced oxygen defects may affect the device performance characteristics such as the device lifetime. This phenomenon should be considered in the models of trapping processes.

1 Introduction

The charge trap flash (CTF) memory, with high-κ film as the charge-capturing layer, is considered as one of the most promising candidates for superseding conventional nonvolatile flash memories, owing to its localized charge storage, low operation voltage, large memory window, and good retention force characteristics. It has received significant attention over the past few decades since the introduction of the metal-nitride-oxide-silicon(MNOS)/polysilicon-oxide-nitride-oxide-silicon (SONOS) concept [1]. Recently, HfO_2 has been proposed as a candidate trapping layer for the CTF, owing to its wide band gap (~5.6 eV), high dielectric constant (~20), and compatibility with the conventional complementary metal oxide semiconductor (CMOS) processing. Understanding the physical mechanisms of the charge-trapping process and the distribution of trapped charges in the CTF is crucial for performance optimization. Using *in situ* electron holography, the charge distribution in the CTF cell structure of metal-Al_2O_3-HfO_2-oxide-silicon was

Address correspondence to Richeng Yu, rcyu@iphy.ac.cn; Ming Liu, liuming@ime.ac.cn

observed directly [2]. The aggregation of negative charge has been characterized near the top of a polycrystalline HfO_2 trapping layer in the CTF sandwich structure. Moreover, positive charges were discovered near the interface between the trapping layer and the tunneling layer. The grain boundary in the polycrystalline HfO_2 trapping layer may serve as a tunnel for the electron transmission to the storage locations [2]. Although much research has been performed to characterize the physical mechanisms of charge trapping, a clear assessment is still lacking. The calculated optical excitation and thermal ionization energies of the oxygen vacancies in the HfO_2 layer, combined with the *C*–*V* and *I*–*V* measurements, indicate that the oxygen vacancies serve as the major charge-trapping sites in HfO_2 [3–8]. In addition, the electrical and reliability characteristics of HfO_2 are often primarily influenced by the oxygen vacancies, owing to the formation of defect states in the band gap [3, 9–15]; these defect sites are generated during the fabrication and annealing processes. However, the detailed conclusions from the calculations and measurements are different. S. K. Sahoo et al. [6] concluded that doubly charged oxygen vacancies serve as the active electron traps, contributing to the leakage current in the gate stacks, while E. A. Choi et al. [7] found that neutral oxygen vacancies may underlie the gate leakage current. The difference may arise from the different calculation methods used by these researchers and from the absence of spatial resolution in the common electrical *I*–*V* and *C*–*V* measurements, which are likely to be affected by the test environment and other parameters. Interestingly, for another HfO_2-based memory-resistive random access memory (RRAM) design, with a sandwich structure similar to that of the CTF, it was proposed that the generation and transport of oxygen vacancies can explain the resistance switching (RS) behavior between the low and high resistance states. [16–22]. The generally accepted RS mechanism in the HfO_2-based RRAM posits that the oxygen vacancies emerging at the top interface drift into the HfO_x layer to form conducting paths during the SET process, and then drift back and accumulate near the top interface to rupture the conducting paths during the RESET process [16–22]. Although the working principles are different, a reasonable speculation is, similar to RRAM, whether a bias could induce oxygen vacancies in the CTF. However, up to this day, the variation of oxygen content under the action of bias has not been observed directly in either the HfO_2-based CTF or RRAM.

In this work, *in situ* electron energy-loss spectroscopy (EELS), combined with the low-loss energy-filtered image in transmission electron microscopy (TEM), was applied to investigate the electronic structure transition process in the HfO_2 layer during the charge-trapping process, which can directly yield the variation of the oxygen content. *In situ* TEM can be used to simultaneously study the microstructures and physical properties of materials, and has been widely used to investigate the CTF and RRAM [2, 23–26]. EELS spectra are sensitive to a change in the electronic state and chemical bonding, while the low-loss energy-filtered images can indicate the location at which the change happens. These techniques could be used to profile the changes in the electronic structure of the HfO_2 trapping layer for different bias values.

2 Results and discussion

2.1 Structural characterization of CTF

Figure 1(a) shows the annular dark-field (ADF) image of a CTF cross-section sample fabricated by using focused ion beam (FIB) technology, in which the multilayer stacks are clearly seen. The fast Fourier transform (FFT) pattern of the high-resolution TEM image (HRTEM) of the HfO_2 layer (inset in Fig. 1(b)) shows that the HfO_2 layer is polycrystalline ($P2_1/c$, a = 5.117 Å, b = 5.175 Å, c = 5.291 Å, α = 90°, β = 99.216°, γ = 90°).

2.2 *In situ* observation of EELS and low-loss energy-filtered image

To investigate the changes in the electronic structure of the HfO_2 film during the programming process, the low energy loss spectra of EELS were recorded at the center of the HfO_2 film, while different positive biases were applied to the gate (Fig. 2). In general, we observed five peaks at 16.4, 26, 35, 37, and 46.4 eV, in the low energy loss spectrum of the HfO_2 film; in

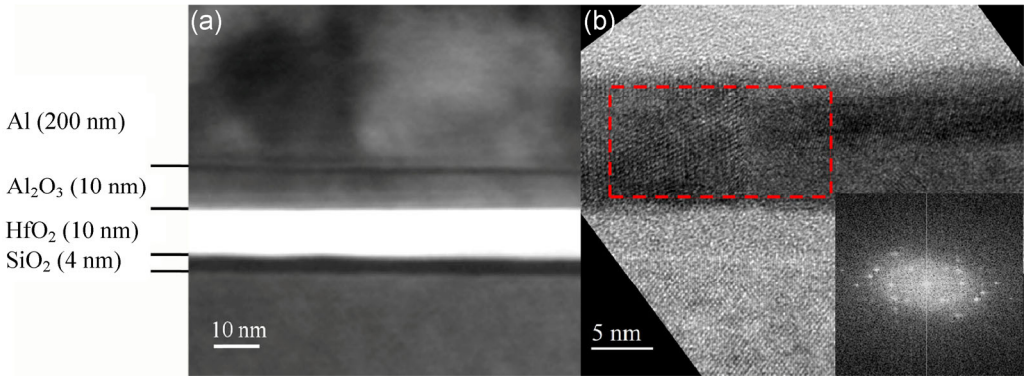

Figure 1 (a) ADF image of the CTF sample cross-section. (b) HRTEM image of the HfO_2 layer. The inset to (b) shows the FFT pattern of the HfO_2 layer.

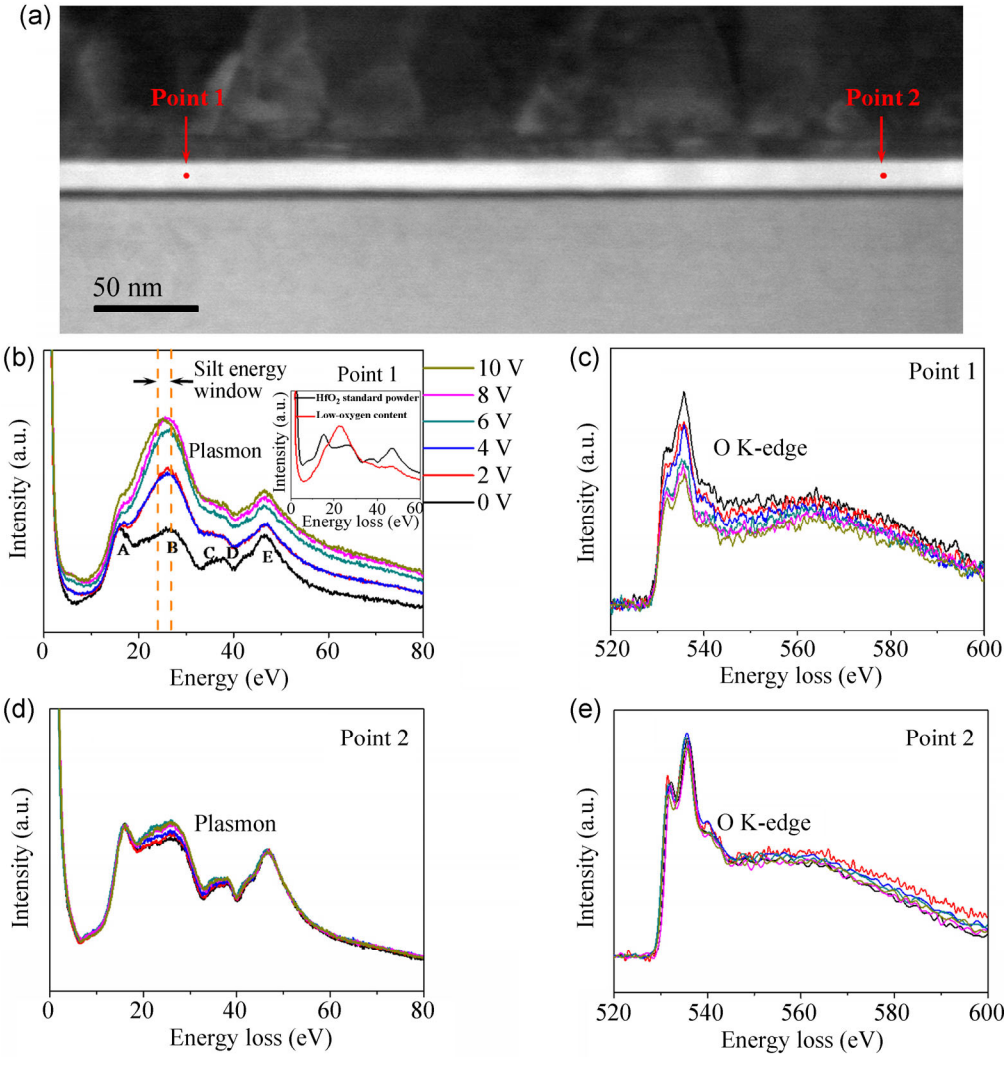

Figure 2 (a) ADF image of the CTF sample. (b) Plasmon loss spectra. (c) Corresponding core-loss EELS spectra of the O K-edge at Point 1, under increased positive bias. (d) Plasmon loss spectra. (e) Corresponding core-loss EELS spectra of the O K-edge at Point 2, under increased positive bias.

Fig. 2 these peaks are labeled as A–E, respectively. Plasmon loss spectrum at zero bias is consistent with that of the standard powder HfO_2 [13]. The theoretical low-loss EELS spectrum of the HfO_2 indicates that the peak A corresponds to the valence plasmon excitation, while the peak B corresponds to the O 2s to Hf 5d excitation [27–29].

The variations in the low energy loss spectra are non-uniformly distributed throughout the HfO_2 film for the same positive gate bias, as shown in Fig. 2. The EELS spectra have been normalized by the zero peak intensity to demonstrate this non-uniformity (Figs. 2(b) and 2(d)). The intensity of peak B increases quickly and the position of peak B moves toward the lower energy region (red shift) with increasing positive bias at Point 1, while the spectrum almost retains the original feature at Point 2 even though the bias increases to 10 V. The peaks in the low energy loss spectrum of the HfO_2 film were reported to be sensitive to the oxygen concentration in the hafnia film. For example, the intensity of peak B should increase relative to that of peak A in a HfO_2 sample with low oxygen content [13]. Thus, the relative difference between the two peak intensities could be used for the characterization of the oxygen consumption in the storage layer. Increasing peak B intensity implies oxygen dissipation, or generation of the oxygen vacancies. This can be confirmed by analyzing the plasmon loss spectra collected from the HfO_2 films with different oxygen contents; this analysis is shown in the supporting information (Fig. S1 in the Electronic Supplementary Material (ESM)). However, we observed that the generation of the oxygen vacancies did not occur uniformly throughout the hafnia layer. For example, the concentration of oxygen varies strongly at Point 1, but exhibits little variation at Point 2. To simplify the discussion, the former position was defined as type-I and the latter as type-II. To figure the variations in the oxygen concentration, the O *K*-edges at both points were acquired under the same bias and the normalized spectra are shown in Figs. 2 (c) and 2(e). For Point 1, the intensity of the entire O *K*-edge decreased when the bias increased, implying the decreasing amount of oxygen. In contrast, the O *K*-edges obtained at Point 2 were almost the same for different bias levels, coincident with the tendency of low energy loss spectra. These results suggest that the oxygen concentration could be easily modulated by applying a positive gate bias at the type-I position but could not be affected at the type-II position.

Moreover, the normalized intensities of peak B, acquired in twenty experiments, were used for characterization of the oxygen concentration variation in the HfO_2 film under different gate biases, and spectral intensity at 0 V was subtracted as a background (Fig. 3). Spectral intensity was integrated in the 18.7–33.1 eV energy window to cover the features of peak B. The gate current density, but not the gate bias, was set as the *X*-axis while comparing between the different sets of experimental data, to minimize the influence of the contact resistance. The current density cannot be detected at a low bias when it is smaller than the detection limit of the *in situ* holder. A typical *I*–*V* curve for the CTF sample, detected by the *in situ* holder, is shown in the supporting information (Fig. S2 in the ESM), which demonstrates that the current is below 1 nA when the bias is below 8 V. However, it should be emphasized that even for a low bias, the oxygen content significantly varies throughout many investigated areas (Fig. 3), which is manifested as the apparent variation in the integrated area under peak B even if there is no measurable current under positive bias. The spatial non-uniformity of oxygen content was reproduced at those twenty detected positions.

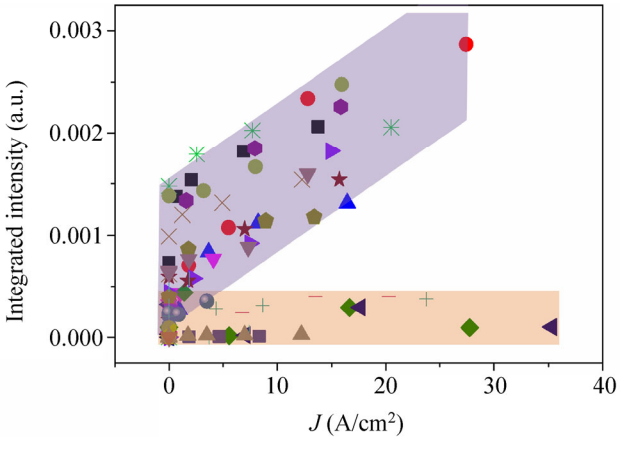

Figure 3 Distribution of the variation of the integrated area under peak B, as a function of the current density. Symbols correspond to the data from different experiments, and the 0 V intensity has been subtracted for each data group. (The grey blue strip summarizes the type I points and the grey pink stripe includes the type II points.)

In Fig. 3, some data points are distributed along the *X*-axis, which means the oxygen content changes little at these type-II like positions. Most of the data points in Fig. 3 are scattered in the left top corner of the map, implying that there may be a possible correlation between the oxygen vacancies and the gate leakage current at those type-I positions.

To trace the influence of bias on the generation of the oxygen vacancies, the plasmon loss spectra in the HfO_2 layer were monitored during both programming and erasing processes. The bias increased from 0 to 10 V and then decreased to –10 V (Fig. 4(a)). The integrated intensity under peak B is plotted in Fig. 4(b). The plot reveals the emergence and increase in the number of the oxygen vacancies with the increasing positive bias and the reduction with the decreasing positive bias. However, for the negative bias the integrated intensity remained nearly unchanged. This implies that the oxygen content may partially recover after the programming is completed, yet leaving a certain number of the oxygen vacancies in the trapping layer. In addition, it seems that the process of erasing does not alter the oxygen concentration. Thus, new oxygen vacancies may be induced only by the programming operation.

The low-loss energy-filtered images of the HfO_2 film were acquired in the TEM mode for mapping the details of the spatially non-uniform distributions of oxygen under different biases (Fig. 5). Because the position of peak B moves from 26 to 24 eV with increasing the positive bias, the energy loss center is fixed at 25 eV. The energy window of the filtered images is 2 eV (indicated in Fig. 2(b)), to avoid the disturbance of the plasmon peaks of Al_2O_3 and SiO_2 (~23 eV). The energy-filtered images reveal the gradual generation and disappearance of the non-uniformly distributed oxygen vacancies, consistent with the results from the plasmon loss spectra. As the bias returns to zero, most locations exhibit residual oxygen vacancies, especially near the interface between the HfO_2 and SiO_2 films.

2.3 Discussion

The generation of oxygen vacancies in the high-κ oxide layer under electric potential is a general phenomenon in many oxide multi-layer structures [16–26, 30–34]. *In situ* EELS characterization also confirmed that the oxygen content could be modulated in the $SrTiO_3/LaAlO_3$ system by applying an external bias [23]. For the HfO_2-based resistive switch memory, it is assumed that the external bias can be used to dissociate the Hf–O bands and induce additional oxygen vacancies, forming the conductive filament (CF) in the HfO_2 film [16–22] (the voltage of the forming process reaches 20 V [18]). Here, for a CTF structure, the plasmon loss spectra, core-loss O *K*-edges and low-loss energy-filtered images confirmed that the concentration of the oxygen vacancies in the HfO_2 film increases when the voltage increases from 0 to 10 V. Owing to their lower activation energy of 0.3 eV [18], the oxygen ions diffuse more efficiently than the

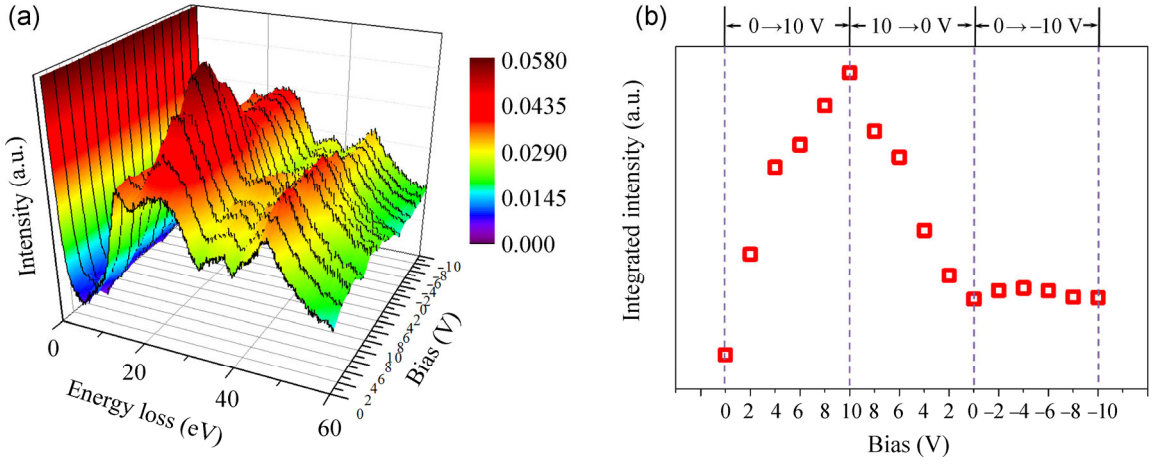

Figure 4 (a) Variation of the EELS vs. the bias. The intensities have been normalized with respect to the intensity at zero. (b) The variation of the integrated area under peak B, vs. the bias. The 0 V intensity has been subtracted.

oxygen vacancies (for V^+ and V^{2+}, the activation energies are 1.2 and 0.7 eV, respectively) in the crystalline HfO_2, thus leaving the vacancies at their original sites. The mechanism of the oxygen concentration recovery in the HfO_2 film remains unclear at the moment. One hypothesis posits that, because the partial potential applied to the HfO_2 layer in the CTF is only several volts, most of the diffusing O^- ions are likely to leave their original sites but will not diffuse far away, while the external bias prevents the recombination of the oxygen ions and the vacancies. For a weaker positive bias, the oxygen ions can recombine with the vacancies, demonstrating the EELS recovery behavior. Considering the complex environment in the trapping layer, the recovery is not complete; thus, there remain some residual oxygen vacancies. These remaining oxygen vacancies may affect the subsequent erasing and programming performance of the device. These induced oxygen vacancies may represent the positive charge that gradually accumulates near the interface between the trapping and tunneling layers during the programming process, as revealed by *in situ* electron holography [2].

Oxygen vacancies in the monoclinic HfO_2 may exist in five charge states (q = –2, ⋯ +2), for which the formation energies are approximate [8, 15]. The negatively charged oxygen vacancies are identified as the major charge-trapping sites in the HfO_2 [6, 8]. In our experiments, the charge states of the oxygen vacancies could not be detected by the plasmon loss spectra, core-loss O *K*-edges and low-loss energy-filtered images. The oxygen vacancies generated during the programming process were distributed throughout the entire HfO_2 charge-trapping layer (shown in the low-loss energy-filtered images of the CTF under 10 V in Fig. 5), while the location of the negative charge aggregation has been directly observed near the top of the polycrystalline HfO_2 charge-trapping layer [2]. This divergence implies that the location of the trapped electrons during the programming process is determined not only by the distribution of the oxygen vacancies, and additional factors should be considered when developing detailed models of charge trapping.

Furthermore, the bias-induced oxygen vacancies may increase the leakage current and shorten the device lifetime [35–41]. Oxygen vacancies were assumed to affect the CTF *I*–*V* performance in a similar way [37–41], but the process was observed here for the first time. The experimental results also suggest that additional information, including the material electrochemical

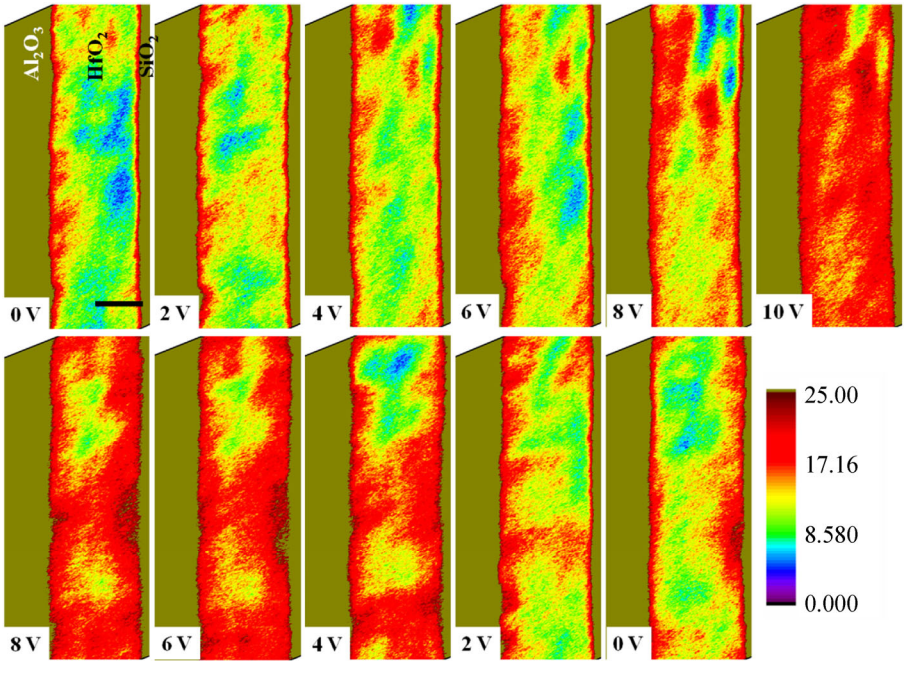

Figure 5 Low-loss energy-filtered images of CTF for different biases, demonstrating that the concentration of the oxygen vacancies increases with the increasing positive bias. The scale bar is 5 nm. (Red encodes higher concentration of the oxygen vacancies.)

characteristics, should be incorporated into the accurate CTF models.

3 Conclusions

In summary, *in situ* TEM observations were performed for $Al/Al_2O_3/HfO_2/SiO_x/Si$ with applied electric fields. The plasmon loss spectra, core-loss EELS spectra of O *K*-edges and low-loss energy-filtered images of the HfO_2 film all indicate that the oxygen content changes during the trapping process. New oxygen vacancies are generated in the HfO_2 film when the positive bias is applied gradually. These results differ from the previous understanding regarding the physical mechanisms of charge trapping in the CTF, which assumed that the defects (such as hafnium vacancies and oxygen-related defects) in the HfO_2 films are generated only during the growth and annealing processes. Significant generation of oxygen vacancies during the programming process should be accounted for in the future models.

4 Experimental

4.1 Devices fabrication

The HfO_2-based CTF sample was prepared as follows. A 4-nm-thick SiO_2 film, acting as the tunneling layer, was thermally grown in dry O_2 ambience on p-type Si (100) wafers. Two layers of Al_2O_3 and HfO_2, each 10-nm-thick, were deposited sequentially on the SiO_2 film by atomic layer deposition at a substrate temperature of 250 ℃. Post-deposition annealing process was conducted in the N_2 ambient conditions under 700 ℃, for 1 min. Finally, a 200-nm-thick Al gate electrode was formed in a lift-off process.

4.2 TEM sample preparation

Preparation of the sandwich CTF samples was described in the previous report [2]. The cross-section CTF samples were mechanically milled to the thickness of ~10 μm and then cut by using the FIB technique with ±2° refinement, to guarantee uniform thickness. Additional 20-s-long Ar ion milling was performed to remove the surface amorphous layers and the possible dead layers. The thickness of the final TEM specimen was ~50 nm, as measured by using the EELS technique, and the results are shown in Fig. S3 (in the ESM) [42]. The sample was loaded on a Nanofactory *in situ* holder, in which an Au tip could be used for applying the voltage to the Al gate of the sample and simultaneously monitoring the current.

4.3 TEM observations

Conventional HRTEM, ADF, low-loss energy-filtered imaging, and EELS were performed by using a field-emission gun TEM (FEI Tecnai F20). The probe size for the EELS and ADF acquisitions was ~10 Å. The EELS spectra were recorded by using the Gatan image filter (Model 794). The energy resolution (full width at half maximum of zero-loss peak) was ~1 eV. Although the low energy loss EELS was featured in detail, the O K-edges were also recorded to monitor the oxygen variation.

Acknowledgements

This work was supported by the National Basic Research Program of China (Nos. 2012CB932302, 2010CB934202 and 2013CB932904), the National Natural Science Foundation of China (No. 10974235).

Electronic Supplementary Material: Supplementary material (EDX and EELS results of different samples synthesized under different oxygen pressures, *I–V* curve of CTF, the low loss spectrum of HfO_2 film and SEM image of the FIB prepared samples) is available in the online version of this article at http://dx.doi.org/10.1007/s12274-015-0857-0.

References

[1] Wegener, H. A. R.; Lincoln, A. J.; Pao, H. C.; O'Connell, M. R.; Oleksiak, R. E.; Lawrence, H. The variable threshold transistor, a new electrically-alterable, non-destructive read-only storage device. In *1967 International Electron Devices Meeting*, Washington, DC, USA, 1967, pp 70.

[2] Yao, Y.; Li, C.; Huo, Z. L.; Liu, M.; Zhu, C. X.; Gu, C. Z.; Duan, X. F.; Wang, Y. G.; Gu, L.; Yu, R. C. *In situ* electron holography study of charge distribution in high-κ charge-trapping memory. *Nat. Commun.* **2013**, *4*, 2764.

[3] Xiong, K.; Robertson, J.; Gibson, M. C.; Clark, S. J. Defect energy levels in HfO_2 high-dielectric-constant gate oxide. *Appl. Phys. Lett.* **2005**, *87*, 183505.

[4] Shockley, W.; Read, W. T. Statistics of the recombinations of holes and electrons. *Phys. Rev.* **1952**, *87*, 835–842.

[5] Park, H.; Jo, M.; Choi, H.; Hasan, M.; Choi, R.; Kirsch, P. D.; Kang, C. Y.; Lee, B. H.; Kim, T. W.; Lee, T. et al. The effect of nanoscale nonuniformity of oxygen vacancy on electrical and reliability characteristics of HfO_2 MOSFET devices. *IEEE Electr. Dev. Lett.* **2008**, *29*, 54–56.

[6] Sahoo, S. K.; Misra, D. Interfacial layer growth condition dependent carrier transport mechanisms in HfO_2/SiO_2 gate stacks. *Appl. Phys. Lett.* **2012**, *100*, 232903.

[7] Choi, E. A.; Chang, K. J. Charge-transition levels of oxygen vacancy as the origin of device instability in HfO_2 gate stacks through quasiparticle energy calculations. *Appl. Phys. Lett.* **2009**, *94*, 122901.

[8] Gavartin, J. L.; Ramo, D. M.; Shluger, A. L.; Bersuker, G.; Lee, B. H. Negative oxygen vacancies in HfO_2 as charge traps in high-κ stacks. *Appl. Phys. Lett.* **2006**, *89*, 082908.

[9] Cho, D. Y.; Lee, Y. J. M.; Oh, S. J.; Jang, H.; Kim, J. Y.; Park, J. H.; Tanaka, A. Influence of oxygen vacancies on the electronic structure of HfO_2 films. *Phys. Rev. B* **2007**, *76*, 165411.

[10] Perevalov, T. V.; Aliev, V. Sh.; Gritsenko, V. A.; Saraev, A. A.; Kaichev, V. V. Electronic structure of oxygen vacancies in hafnium oxide. *Microelectron. Eng.* **2013**, *109*, 21–23.

[11] Zhang, W.; Hou, Z. F. Interaction and electronic structures of oxygen divacancy in HfO_2. *Phys. Stat. Sol. (b)* **2013**, *250*, 352–355.

[12] Pandey, R. K.; Sathiyanarayanan, R.; Kwon, U.; Narayanan, V; Murali, K. V. R. M. Role of point defects and HfO_2/TiN interface stoichiometry on effective work function modulation in ultra-scaled complementary metal-oxide-semiconductor devices. *J. Appl. Phys.* **2013**, *114*, 034505.

[13] Jang, J. H.; Jung, H. S.; Kim, J. H.; Lee, S. Y.; Hwang, C. S.; Kim, M. Investigation of oxygen-related defects and the electrical properties of atomic layer deposited HfO_2 films using electron energy-loss spectroscopy. *J. Appl. Phys.* **2011**, *109*, 023718.

[14] Jo, M.; Park, H.; Chang, M.; Jung, H. S.; Lee, J. H.; Hwang, H. Oxygen vacancy induced charge trapping and positive bias temperature instability in HfO_2 nMOSFET. *Microelectron. Eng.* **2007**, *84*, 1934–1937.

[15] Broqvist, P.; Pasquarello, A. Oxygen vacancy in monoclinic HfO_2: A consistent interpretation of trap assisted conduction, direct electron injection, and optical absorption experiments. *Appl. Phys. Lett.* **2006**, *89*, 262904.

[16] Bersuker, G.; Gilmer, D. C.; Veksler, D.; Kirsch, P.; Vandelli, L.; Padovani, A.; Larcher, L.; McKenna, K.; Shluger, A.; Iglesias, V. et al. Metal oxide resistive memory switching mechanism based on conductive filament properties. *J. Appl. Phys.* **2011**, *110*, 124518.

[17] Yu, S. M.; Gao, B.; Dai, H. B.; Sun, B.; Liu, L. F.; Liu, X. Y.; Han, R. Q.; Kang, J. F.; Yu, B. Improved uniformity of resistive switching behaviors in HfO_2 thin films with embedded Al layers. *Electrochem. Solid-St. Lett.* **2010**, *13*, H36–H38.

[18] Tran, X. A.; Zhu, W.; Liu, W. J.; Yeo, Y. C.; Nguyen, B. Y.; Yu, H. Y. Self-selection unipolar HfO_x-based RRAM. *IEEE Trans. Electr. Dev.* **2013**, *60*, 391–395.

[19] Chen, Y. Y.; Goux, L.; Clima, S.; Govoreanu, B.; Degraeve, R.; Kar, G. S.; Fantini, A.; Groeseneken, G.; Wouters, D. J.; Jurczak, M. Endurance/retention trade-off on cap 1T1R bipolar RRAM. *IEEE Trans. Electr. Dev.* **2013,** *60*, 1114–1121.

[20] Lin, Y. S.; Zeng, F.; Tang, S. G.; Liu, H. Y.; Chen, C.; Gao, S.; Wang, Y. G.; Pan, F. Resistive switching mechanisms relating to oxygen vacancies migration in both interfaces in Ti/HfO_x/Pt memory devices. *J. Appl. Phys.* **2013**, *113*, 064510.

[21] Zhang, H. W.; Liu, L. F.; Gao, B.; Qiu, Y. J.; Liu, X. Y.; Lu, J.; Han, R.; Kang, J. F.; Yu, B. Gd-doping effect on performance of HfO_2 based resistive switching memory devices using implantation approach. *Appl. Phys. Lett.* **2011**, *98*, 042105.

[22] Lee, J.; Bourim, E. M.; Lee, W.; Park, J.; Jo, M.; Jung, S.; Shin, J.; Hwang, H. Effect of ZrO_x/HfO_x bilayer structure on switching uniformity and reliability in nonvolatile memory applications. *Appl. Phys. Lett.* **2010**, *97*, 172105.

[23] Yang, Y.; Lü, W. M.; Yao, Y.; Sun, J. R.; Gu, C. Z.; Gu, L.; Wang, Y. G.; Duan, X. F.; Yu, R. C. *In situ* TEM observation of resistance switching in titanate based device. *Sci. Rep.* **2013**, *4*, 3890.

[24] Kwon, D. H.; Kim, K. M.; Jang, J. H.; Jeon, J. M.; Lee, M. H.; Kim, G. H.; Li, X. S.; Park, G. S.; Lee, B.; Han, S. et al. Atomic structure of conducting nanofilaments in TiO_2 resistive switching memory. *Nat. Nanotechnol.* **2010**, *5*, 148–153.

[25] Park, G. S.; Kim, Y. B.; Park, S. Y.; Li, X. S.; Heo, S.; Lee, M. J.; Chang, M.; Kwon, J. H.; Kim, M.; Chung, U. I. et al. *In situ* observation of filamentary conducting channels in an asymmetric Ta_2O_{5-x}/TaO_{2-x} bilayer structure. *Nat. Commun.* **2013**, *4*, 2382.

[26] Liu, Q.; Sun, J.; Lv, H. B.; Long, S. B.; Yin, K. B.; Wan, N.; Li, Y. T.; Sun, L. T.; Liu, M. Real-time observation on dynamic growth/dissolution of conductive filaments in oxide-electrolyte-based ReRAM. *Adv. Mater.* **2012**, *24*, 1844–1849.

[27] Guedj, C.; Hung, L.; Zobelli, A.; Blaise, P.; Sottile, F.; Olevano, V. Evidence for anisotropic dielectric properties of monoclinic hafnia using valence electron energy-loss spectroscopy in high-resolution transmission electron microscopy and *ab initio* time-dependent density-functional theory. *Appl. Phys. Lett.* **2014**, *105*, 222904.

[28] Park, J.; Yang, M. Determination of complex dielectric functions at HfO_2/Si interface by using STEM-VEELS. *Micron* **2009**, *40*, 365–369.

[29] Kang, Y. S.; Kim, D. K.; Kang, H. K.; Cho, S.; Choi, S.; Kim, H.; Seo, J. H.; Lee, J.; Cho, M. H. Defect states below the conduction band edge of HfO_2 grown on InP by atomic layer deposition. *J. Phys. Chem. C* **2015**, *119*, 6001–6008.

[30] Sawa, A. Resistive switching in transition metal oxides. *Mater. Today* **2008**, *11*, 28–36.

[31] Bersuker, G.; Yum, J.; Vandelli, L.; Padovani, A.; Larcher, L.; Iglesias, V.; Porti, M.; Nafría, M.; McKenna, K.; Shluger A. et al. Grain boundary-driven leakage path formation in HfO_2 dielectrics. *Solid-State Electron.* **2011**, *65–66*, 146–150.

[32] Lanza, M. A review on resistive switching in high-κ dielectrics: A nanoscale point of view using conductive atomic force microscope. *Materials* **2014**, *7*, 2155–2182.

[33] Broqvist, P.; Pasquarello, A. First principles investigation of defects at interfaces between silicon and amorphous high-κ oxides. *Microelectron. Eng.* **2007**, *84*, 2022–2027.

[34] Zhang, T.; Ou, X.; Zhang, W. F.; Yin, J.; Xia, Y. D.; Liu, Z. G. High-κ-rare-earth-oxide Eu_2O_3 films for transparent resistive random access memory (RRAM) devices. *J. Phys. D: Appl. Phys.* **2014**, *47*, 065302.

[35] Lyons, J. L.; Janotti, A.; Van de Walle, C. G. The role of oxygen-related defects and hydrogen impurities in HfO_2 and ZrO_2. *Microelectron. Eng.* **2011**, *88*, 1452–1456.

[36] Mao, L. F.; Wang, Z. O. First-principles simulations of the leakage current in metal-oxide-semiconductor structures caused by oxygen vacancies in HfO_2 high-κ gate dielectric. *Phys. Stat. Sol. (a)* **2008**, *205*, 199–203.

[37] Nadimi, E.; Roll, G.; Kupke, S.; Öttking, R.; Plänitz, P.; Radehaus, C.; Schreiber, M.; Agaiby, R.; Trentzsch, M.; Knebel, S. et al. The degradation process of high-κ SiO_2/HfO_2 gate-stacks: A combined experimental and first principles investigation. *IEEE Trans. Electr. Dev.* **2014**, *61*, 1278–1283.

[38] Perevalov, T. V.; Gritsenko, V. A. Application and electronic structure of high-permittivity dielectrics. In *Proceedings of the 2010 27th International Conference on Microelectronics Proceedings*, Nis, Serbia, **2010**, pp 123–126.

[39] Padovani, A.; Larcher, L.; Bersuker, G.; Pavan, P. Charge transport and degradation in HfO_2 and HfO_x dielectrics. *IEEE Electr. Dev. Lett.* **2013**, *34*, 680–682.

[40] Mao, L. F.; Wang, Z. O.; Wang, J. Y.; Zhu, C. Y. The conduction band alignment of HfO_2 caused by oxygen vacancies and its effects on the gate leakage current in MOS structures. *Eur. Phys. J. Appl. Phys.* **2007**, *40*, 59–63.

[41] Mannequin, C.; Gonon, P.; Vallée, C.; Latu-Romain, L.; Bsiesy, A.; Grampeix, H.; Salaün, A.; Jousseaume, V. Stress-induced leakage current and trap generation in HfO_2 thin films. *J. Appl. Phys.* **2012**, *112*, 074103.

[42] Egerton, R. F. *Electron Energy-Loss Spectroscopy in the Electron Microscope*; Springer: New York, USA, 1995.